P6.18 **SSMIS LOWER ATMOSPHERIC SOUNDING CAL/VAL**

Donald Boucher,* Robert Farley,* Al Fote,* Ye Hong,* Dave Kunkee,* Gene Poe,**
Steve Swadley,** Bruce Thomas,* and John Wessel*

*The Aerospace Corporation
**Naval Research Laboratory

1. INTRODUCTION AND BACKGROUND

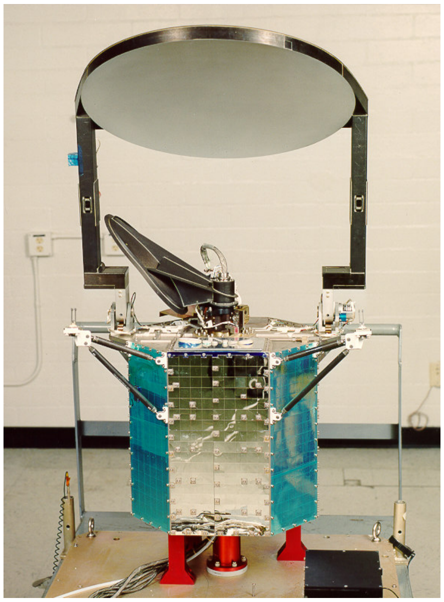

Figure 1. SSMIS prior to deployment.

This report describes calibration of the DMSP Special Sensor Microwave Imager Sounder (SSMIS) Lower Atmospheric Sounding (LAS) channels. SSMIS, shown in Figure 1, is a conically scanning microwave imager/sounder. It combines the functionality of SSM/I together with a number of new sounding features providing vastly increased altitude coverage, based on new 60 GHz oxygen channels for mesospheric temperature profiling. The conical scan geometry provides uniform imaging and weighting functions (Figure 2), as opposed to varying weighting functions and polarization for conventional cross-track instruments. Higher spatial resolution, relative to SSM/T-1 and SSM/T-2, is available in sounding channels. The 19-92 GHz surface channels functionally duplicate SSM/I and the instrument architecture resembles SSM/I. The moisture channel frequencies coincide with SSM/T-2. The instrument body and main reflector rotate together and the reflector is external to warm load and cold sky calibration pathways. Many aspects of calibration will be discussed elsewhere. These include calibration of SSM/I-related channels (12-18) and Upper Atmsopheric Sounding (UAS) channels (19-24). Extensive efforts performed by NRL led to high quality data for SSM/I-related imaging channels. Those efforts also included readjustment of geolocation parameters and improvement of antenna pattern corrections.

Corresponding author: john.e.wessel@aero.org

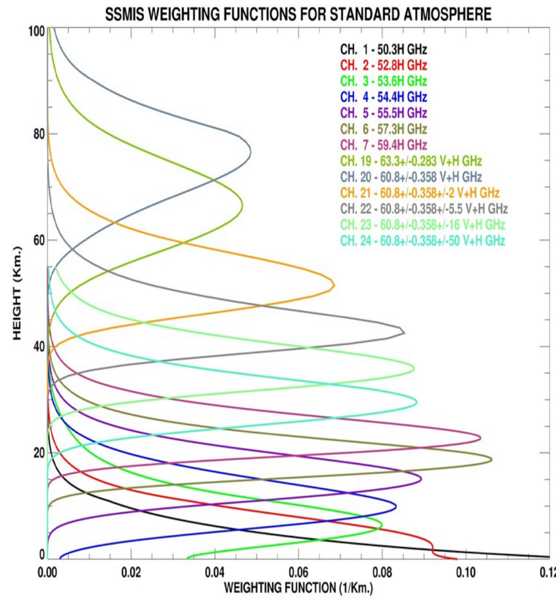

f

Figure 2. Temperature sounding channel weighting functions for a standard atmosphere.

Currently, UAS channels are operating nominally and there is satisfactory agreement between the SDRs and simulated brightness temperatures calculated from lidar temperature profiles.

This report does not address validation of environmental data record (EDRs) retrievals. Corrections for LAS sounding channel bias are not finalized, therefore it is too early to assess EDR accuracy. Comparisons performed to date based on available SDRs indicate temperature retrievals generally meet DMSP requirements, whereas relative humidity retrieval errors are significant for several atmosphere types

SSMIS LAS on-orbit calibration is primarily based on comparisons between SSMIS SDRs and radiative transfer calculations performed using atmospheric temperature and water vapor profiles derived from operational radiosondes, ECMWF fields, and lidar measurements. The rational for choice of ground truth is based on the following considerations. Operational radiosonde reports have relatively good geographical distribution, they provide multiple independent physical measurements and therefore, they are presumably less subject to bias than NWP. A subset of synoptic measurements is timely relative to F-16 overpasses. NWP fields provide full geographical coverage, they effectively suppress noise associated with individual radiosonde measurements, and the profiles extend above typical radiosonde ceilings. Dedicated lidar measurements of water vapor and temperature profiles provide high accuracy, high altitude capability, exact time coincidence, and definitive cloud measurements. However, lidar campaigns were geographically restricted and of short duration. The radiative transfer calculations were performed using the in-house program, CMRT, which employs the Rosenkranz (1998) atmospheric transmission model. Cross comparisons were run between CMRT, RTTOVS-6 and in-house radiative transfer programs employed at NRL and Northrop-Grumman Space Systems. Results were in excellent agreement.

This report begins by presenting globally averaged results for 2004 and results from three separate lidar campaigns made in winter 2003, spring 2004, and winter 2004. This is followed by detailed consideration of local and seasonal results, which identified problems involving variable instrument bias. Transient gain anomalies due to solar illumination of the warm calibration load surface are not addressed in this report. Since they are geographically and temporally localized, their influence on the averaged errors discussed below is insignificant.

1.1 Data Archive

SSMIS LAS Cal/Val data acquisition was performed by Aerospace personnel located at AFWA in Omaha, Nebraska. Radiosonde and NWP fields were acquired on a daily basis. The LAS Cal/Val database is organized into daily directories containing soundings that meet quality control (QC) requirements, together with matching SSMIS TDRs, SDRs, EDRs, and NWP fields extracted from the regions surrounding each of the matchup sites. Data are also archived from heritage sensors including SSM/I, SSM/T-1, SSM/T-2, and AMSU. These are used for cross calibration and benchmark studies. The matchup time criterion was set to +/-90 minutes, representing a compromise between data volume requirements and need to minimize atmospheric change between SSMIS observation and ground truth measurements. The horizontal requirement was set to +/-200 km in order to acquire sufficient imagery in the vicinity of each raob site. Operational raob quality control (QC) was performed with an in-house program that was modeled on the program described by Collins (1998). It tests for physically reasonable lapse rates, continuity (reasonable level spacing) of temperature and moisture measurements, hypsometric accuracy, and possible presence of clouds and moisture saturation effects. Approximately 40 percent of operational radiosondes meet QC requirements. The geographic distribution of sounding sites is shown in Figure 3. Matchup locations are limited by the F-16 orbit and by synoptic cycle times of 0 and 12 UT, combined with sampling window requirements.

NRL accumulates global NWP fields, including ECMWF and uses these to monitor SSMIS performance on a global scale. During the prelaunch period, comparisons between ground truth and satellite and lidar measurements led to standardization on ECMWF as the reference NWP field. The database provides time-interpolated analysis fields.

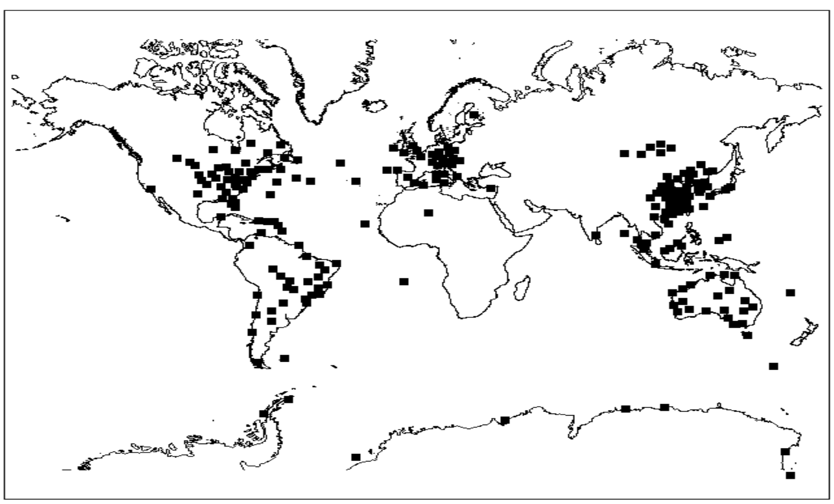

Figure 3. Typical F-16 Cal/Val raob matchup sites.

1.2 Special Observations

Dedicated water vapor and temperature measurements were performed in three lidar campaigns carried out at Barking Sands, Kauai, located in the mid-Pacific at 22.05° N, 159.78° W. In addition, a large number of upper atmospheric temperature profiles were supplied by the JPL lidar group from Table Mountain, California, 34.4°N, 117.7°W, and Mauna Loa, Hawaii, 19.54°N, 155.58°W. The latter are used primarily for UAS Cal/Val.

Special observation campaigns provided dropsonde and radiosonde data. In this section of the report, data are used from flights of the ATOST North Atlantic Dropsonde Campaign on 27 November, 2003, and on 8-

9 December, 2003. (first flight--latitudes 47-52 N, longitudes 15-48 W, and times 10-14 UT, second flight-- latitudes 44-41 N, longitudes 67-63 W, and times 8 December UT 2228 to 9 December 2003, 0040 UT.) Dropsonde data provided by the NOAA Aeronomy Lab are also used from the WSRP mid-Pacific Campaign, 29 Jan 2004, (latitudes 19 N-25 N, longitudes 153 W-157 W, and times 18-20 UT) and from dedicated RS-90 radiosondes launches made in the equatorial Pacific by the NOAA Aeronomy Lab personnel aboard the R. V. Brown, from 27 Oct to 20 Nov 2003 (latitudes between 90 W and 110 W, longitudes from 0N to 12N, and times from 0 to 23 UTC). Results from CoSMIR and APMIR aircraft-based radiometer underflights will be presented elsewhere.

1.3 Ground Truth Characterization

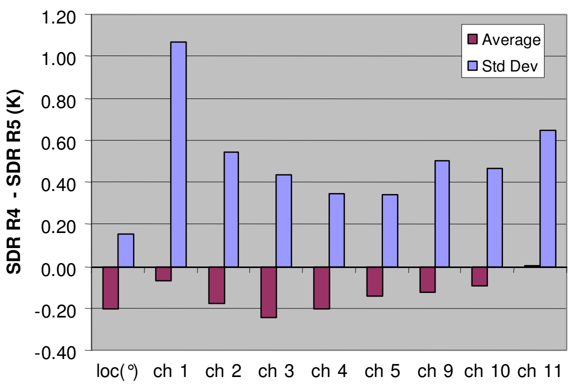

S

Figure 4. F16 SSMIS R4 versus R5 LAS SDRs

SMIS calibration relies on accurate sources of ground truth. Characteristics of the reference sources were assessed at Barking Sands and Arm/Cart SGP using available high accuracy measurement methods. Scientific quality radiosonde (Vaisala RS-90) measurements were compared against NWP and NWS radiosondes. In addition, dedicated lidar temperature and water vapor measurements were used as reference standards. The results indicated that NWP accuracy is somewhat variable as a function of season and location. At the Barking Sands location, NWP errors were typically less than 1 K RMS between the surface and 100 mb. Accuracy degraded at higher altitudes, and ECMWF, which profiles to 1 mb, degrades severely between 7 and 2 mb. NWS raob moisture measurements are reliable at low altitudes and inaccurate at high altitudes. NWP RMS error generally exceeded 1 K at the continental SGP site. We concluded that lidar is required to measure RMS performance for high altitude temperature and moisture channels, given the need to calibrate SDRs to +/-1 K. For low altitudes, excepting the surface, NWP and raobs may be adequate to assess biases. In many cases, NWP and raobs were able to resolve changes in bias as a function of latitude.

1.4 Ground Processing Software And SDR Versions

During Cal/Val, it was determined that ground processing software (Revision 4 GDPS) used to produce SDRs and EDRs (SDRP and EDRP) required modification to correct for geolocation errors, spill-over loss at scan edges, and an instrument polarization error. This led to issue of Revision 5 GDPS. Fortunately, the changes are not significant for purposes of LAS Cal/Val, as discussed below. Revision 4 GDPS was used to process data used in this report, unless otherwise noted. Differences between Rev 4 and Rev 5 format LAS SDRs were surveyed. Results are summarized in Figure 4.

Average SDR offsets are small relative to the derived instrumental radiometric calibration requirement of +/-1 K. Geolocation errors are substantial for pixel-by-pixel imaging, however offsets are negligible when comparing average differences between measured and calculated SDRs. Standard deviations of SDR offsets are larger and may influence final comparison results. The large standard deviation for channel 1 is small relative to the spread in SDRs caused by surface variation.

1.5 Report Outline

Initial calibration results were analyzed without explicitly considering the possibility that instrumental bias varies as a function of orbit, season, and latitude. Later on, changes in bias were observed. Therefore, this report is organized to describe general calibration characteristics, followed by characterization of local effects.

Although studies of varying bias and identification of root causes are now complete, the quantitative bias correction model remains under development. Therefore, this report documents the existence of anomalies, makes recommendations for corrective changes to instrument and software, and explores some aspects of a corrective model.

2. AVERAGE CALIBRATION RESULTS

The following studies emphasize channels 3-5 and 9-11 the surface contributions are minimal and their weighting functions do not extend substantially beyond measurement ceiling altitudes. Calibration errors for channels 1 and 2 are expected to be related to those for channels 3 to 5 because calibration sources and feedhorns are shared. If there are calibration differences, their impact on retrievals is diminished in the presence of larger unaccounted variations associated with surface signals. Calibration of stratospheric LAS channels 6, 7 and UAS channels is primarily addressed by lidar measurements.

Scatter plots of CMRT radiative transfer simulations versus SSMIS Rev 4 SDRs are shown in Figures 5 and 6, where scales are different for each set of measurements. Matchups were made for 2003 Julian day (JD) 306-365, with maximum offset distances of 50 km. Scales vary from chart to chart. Measurements are located in the vicinity of Barking Sands, Kauai. The lidar results suggest significant bias for channel 4. Cloud contamination would decrease SSMIS brightness temperatures.

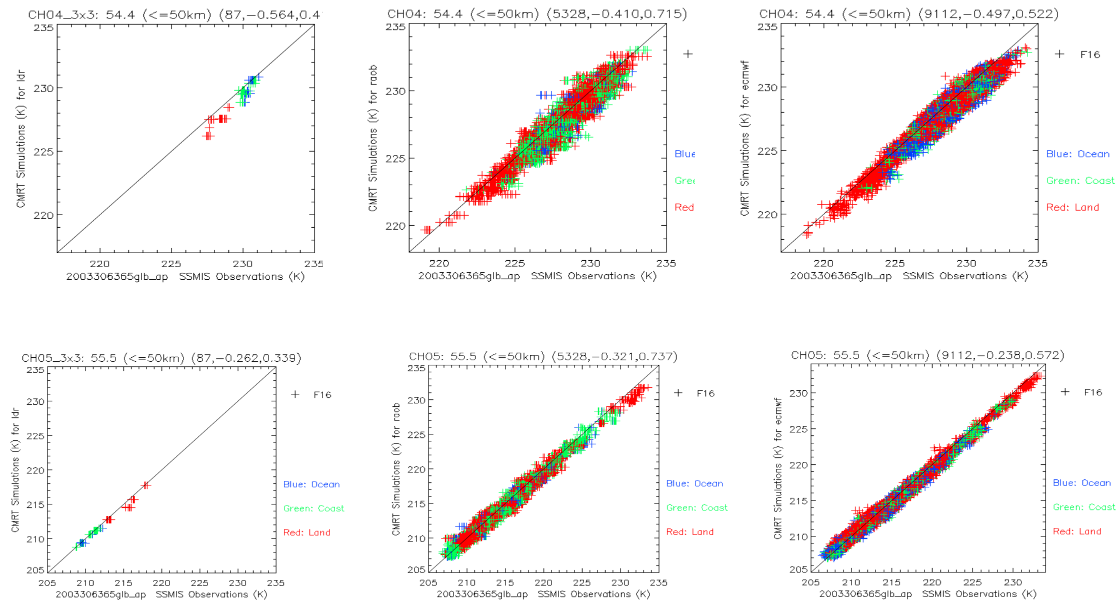

Figure 5. SSMIS scatter plots, winter 2003 temperature sounding. Barking Sands lidar is shown on the left, ECMWF in the middle, and raobs on the right. Blue represents ocean, green coast, and red land.

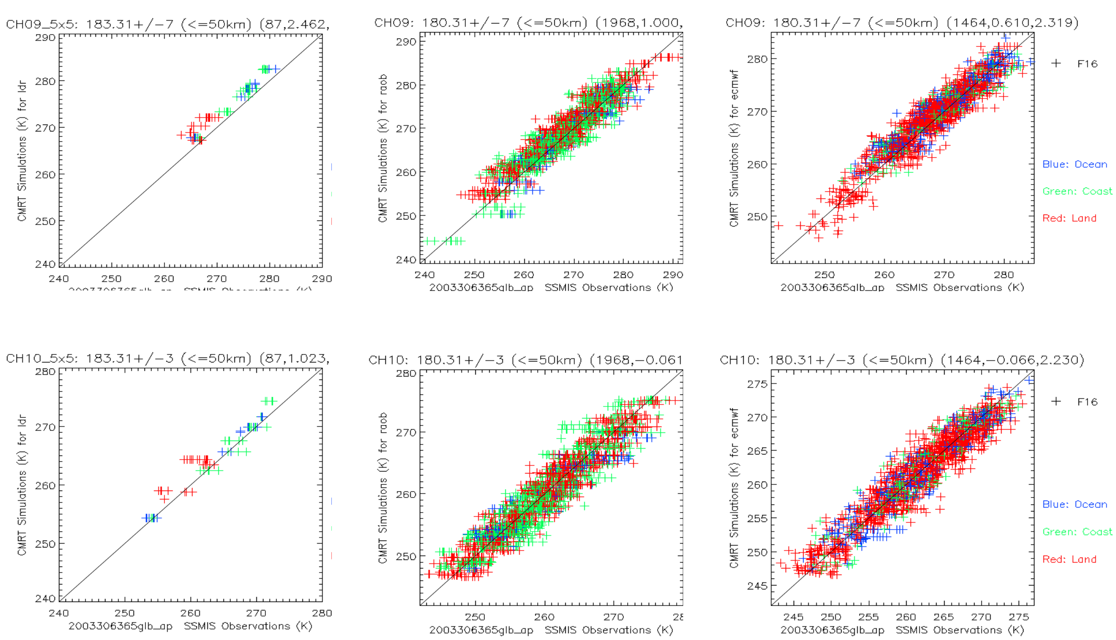

Figure 6. SSMIS scatter plots, winter 2003 water vapor sounding.

Again, lidar results suggest channel 9 is biased, however bias is less apparent in the raob and ECMWF comparisons.

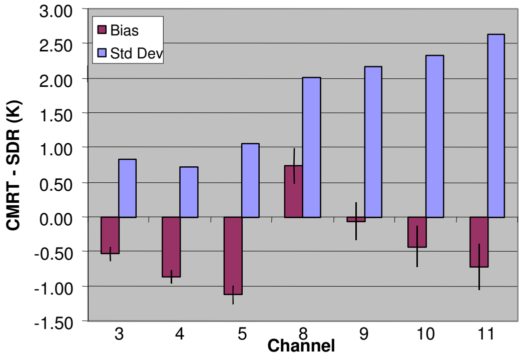

Figure 7. SSMIS bias, standard deviation, and 90% confidence level, global raobs 2004.

2.1 Statistical Results

Figure 7 and Table 1 present statistical results for the global set of operational radiosondes measurements that meet selection criteria. The vertical lines represent statistical uncertainty in the average, calculated for the limited size data set. It is given by the 90% confidence interval of the mean. Results are based on Rev 4 SDRs.

Averaged over the entire year, biases exceeded the 90% confidence level for channels 3, 4, 5, 8, 10, and 11, however they are within the derived requirement of +/-1 K, excepting channel 5, which slightly exceeds requirements. In this case agreement is reasonable, considering statistical error (+/-0.13 K), possible systematic errors in radiative transfer and raob measurements, and differences between the Rev 4 SDRs used above and the corrected Rev 5 SDRs (0.15 K). Standard deviations are large for moisture channels 8-11. This suggests that local bias drifts as a function of location and/or season, that there are ground truth measurement problems, or that there is elevated short term noise in SSMIS SDRs.

3. LIDAR CAMPAIGN RESULTS

Three Cal/Val lidar campaigns were carried out from launch to December, 2004 at Barking Sands, Kauai located at 22.05 N, 159.78 W. The lidar is about 3 m above sea level and the system is optimized for water va por profiling. Vaisala RS-90 radiosondes were launched before each SSMIS overpass. The lidarwas calibrated against average radiosonde measurements and results were checked against known saturated atmospheric conditions. Lidar is used to profile temperatures above the radiosonde ceiling altitudes, which occur at approximately 30 km. The combined lidar—radiosonde measurements provide approximately 10 percent accuracy for relative humidity between the surface and 10 km altitude. Accuracy declines to about 25 percent at about 15 km for the typical averaging period of 20 minutes. RS-90 radiosonde temperatures are accurate to about +/-0.5 K from the surface to above 20 km. Cal/Val profiles are constructed from the merged lidar/RS-90 data and MSIS-90 climatology, Hedin (1991), is used above the lidar ceiling. Reported observations are approximately centered on SSMIS overpass times, unless interfering clouds were present. If they were, offsets up to 30 minutes were permitted in order to acquire lidar data. For altitudes below 8 km, lidar and radiosonde measurements agreed within 10 percent relative humidity. Lidar temperature profiles were uncertain over the range 30-35 km, particularly for the winter 2003 and April 2004 campaigns. Errors could be up to 5 K

Table 1

SSMIS Calibration Statistics
Operational Radiosondes 2004 JD 1 – 365
CDFSII Cloud-Screened

Ch	CMRT-SDR(K)	RMS	90% Conf	Std Dev
3	-0.53	0.98	0.11	0.83
4	-0.86	1.12	0.09	0.72
5	-1.12	1.54	0.13	1.05
8	0.74	2.14	0.26	2.01
9	-0.06	2.17	0.28	2.17
10	-0.43	2.36	0.29	2.32
11	-0.7	2.73	0.33	2.64

Rev 4 SDRs

in this region. Above that, errors decline to less than 2 K, until signals become weak, at about 55 km.

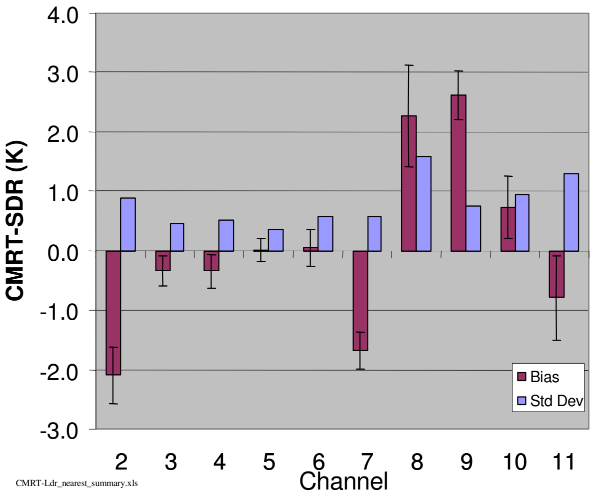

Figure 3. SSMIS bias, standard deviation, and 90% confidence, Barking Sands Lidar, 11/03--1/04

The measurements are more uncertain than climatology above 70 km. In terms of calibration accuracy, water vapor results should support radiative transfer measurements to an accuracy of 1 K, provided the atmospheric transmission model is accurate and local orographic effects do not affect the comparisons. (Channel 9 TDR imagery was examined for evidence of local water vapor variation. No evidence of statistically significant local water vapor variation was detected in the TDRs.) Radiative transfer temperature accuracy should be better than 1 K for channels 3-5, whereas results for 6 and 7 may be degraded to +/-2 K for the earlier measurements and be approximately +/-1K for December 2004. Radiative transfer accuracy for channels 2 and 8 is degraded by uncertainty in surface emissivity.

Barking Sands lidar-based comparisons for winter 2003-2004, derived from 12 nights of observation, are shown in Figure 8 and Table 2. The vertical lines represent 90 percent confidence intervals for bias. (12 overpasses) These results are much different than for the yearly global data set, particularly for water vapor channels 8-11. Lidar indicates unexpectedly large bias for channel 9, together with a low standard deviation. The latter implies that SSMIS is locally stable and both it and the lidar respond similarly to environmental change.

Initially, it was thought that the channel 8 and 9 biases were due to the influence of clouds. CDFSII-based screening (Air Force/DMSP cloud forecasting system) was investigated and a regression of bias versus cloud cover predicted the channel 9 bias declines to 1 K at the zero cloud cover intercept. However, the statistical uncertainty in the intercept is +/-2K. Currently, it is believed that clouds have a negligible influence on the channel 9 SDRs observed near Barking Sands during the 2003-2005 lidar campaigns. Therefore, the biases shown in Figure 8 and Table 2, uncorrected for CDFSII cloud cover, are believed to provide the best estimates.

Systematic errors associated with surface emissivity estimates preclude useful comparisons for channels 1, 2 and 8, which have significant surface contributions. Channel 7 response peaks in the altitude range 30-35 km. The Barking Sands lidar bias uncertainty is +/-2 K or more over this range, therefore biases indicated above are considered to be nominal. Standard deviations are excellent for all channels, considering SSMIS NEΔTs, lidar uncertainties, and horizontal inhomogeneity. The small standard deviations indicate that SSMIS SDRs are locally stable. Although standard deviations for lidar are much smaller than for the global raob data set, the relatively small number of measurements increases uncertainty in bias in comparison to the raob data set.

Table 2, SSMIS Barking Sands Lidar Calibration Results

CMRT – SDR (K), Nov. 2003 – Jan 2004

Channel 2	3	4	5	6	7	8	9	10	11	
Bias	-2.1	-0.3	-0.3	0.0	0.1	-1.7	2.3	2.6	0.7	-0.8
RMS	2.3	0.6	0.6	0.4	0.6	1.8	2.8	2.7	1.2	1.5
Std. Dev.	0.9	0.5	0.5	0.4	0.6	0.6	1.6	0.7	1.0	1.3
90% Conf	0.5	0.3	0.3	0.2	0.3	0.3	0.9	0.4	0.5	0.7

The results in Table 2 summarize the initial lidar calibration obtained during the Nov 2003 – Jan 2004 campaign. Values are calculated using Rev 4 SDRs and no correction is made for cloud coverage.

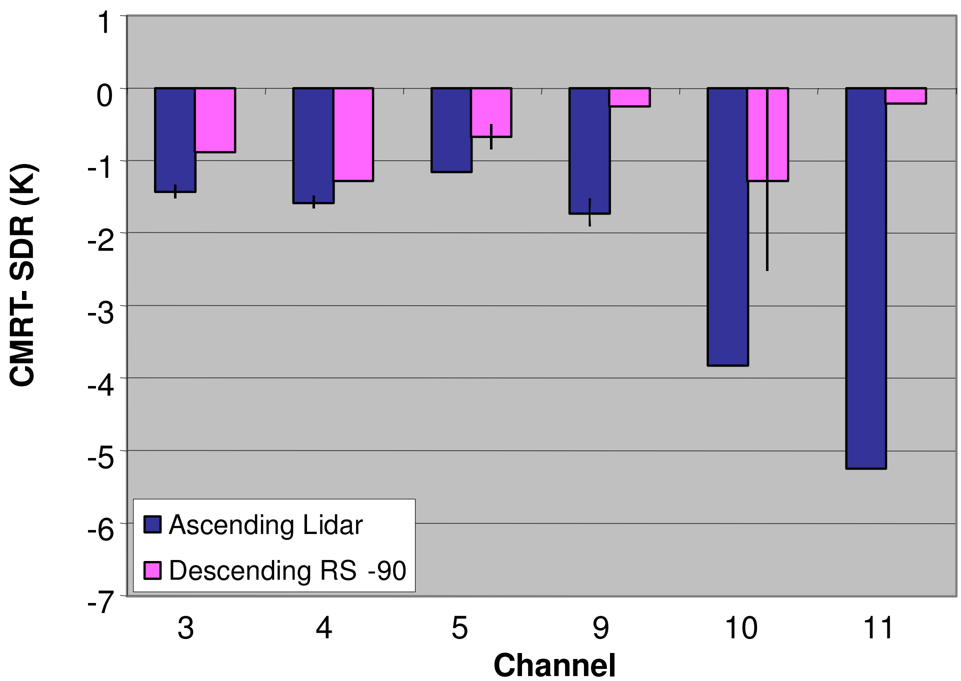

Figure 9. SSMIS Bias, Barking Sands Lidar, April 2004

Table 3. SSMIS Barking Sands Lidar Calibration Results, April 2004

Ascending (Lidar)						
Channel	3	4	5	9	10	11
Bias (K)	-1.42	-1.57	-1.15	-1.72	-3.81	-5.24
RMS	1.43	1.58	1.16	1.76	3.97	5.39
Std Dev	0.17	0.16	0.17	0.39	1.13	1.29
90% Conf	0.09	0.08	0.09	0.20	0.58	0.66
Descending (RS-90)						
Bias (K)	-0.90	-1.24	-0.71	-0.23	-1.27	-0.14
RMS	0.94	1.26	0.74	0.80	2.02	0.77
Std Dev	0.27	0.23	0.21	0.77	1.58	0.75
90% Conf	0.22	0.18	0.17	0.61	1.25	0.60

Except for the cases of channels 5 and 11, ascending CMRT results are expected to be essentially identical for lidar and for RS-90 profiles.

A second campaign was conducted in April, 2004. Biases and RMS, shown in Figure 9 and tabulated in Table 3, were much different than observed in winter 2003, greatly exceeding statistical and ground truth uncertainties.

A third lidar campaign was performed in December, 2004. Ascending orbit biases are shown in Figure 10 and statistics are tabulated in Table 4. Results were essentially the same as those for the winter 2003 campaign, indicating that bias changes are reproducible on a yearly basis, even though seasonal changes are large.

Table 4. SSMIS Barking Sands, Calibration Results, Lidar, Ascending Dec 2004

Channel	2	3	4	5	6	7	8	9	10	11
Bias (K)	-0.11	-0.39	-0.54	0.00	-0.05	-1.21	1.55	2.41	1.03	0.45
RMS	0.39	0.56	0.68	0.46	0.53	1.40	2.94	2.62	1.32	1.16
Std Dev	0.37	0.40	0.41	0.46	0.53	0.69	2.50	1.01	0.83	1.07
90% Conf	0.14	0.15	0.15	0.17	0.19	0.25	0.92	0.37	0.30	0.39

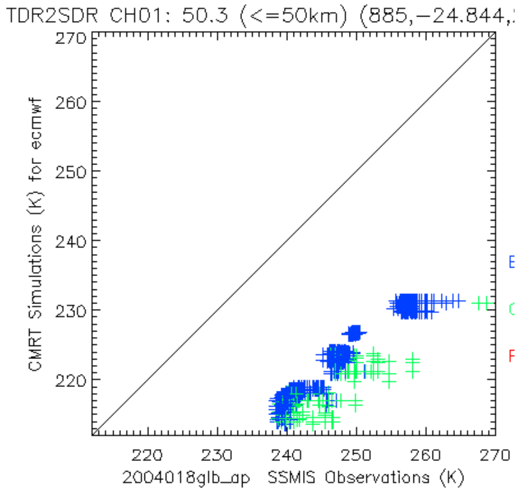

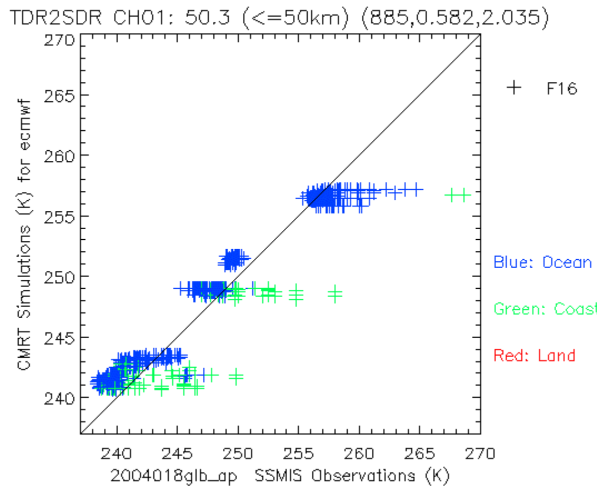

Figure 10. Ch l , CMRT(H-pol) Versus SDR.

Figure 11. Channel 1, CMRT(V-pol) Versus SDR. 45 S-45 N cloud-free ocean/coast, 18 April. 2004.

4. CHANNEL 1 AND CHANNEL 2 POLARIZATION DISCREPANCIES

CoSMIR underflights of SSMIS performed in March and April, 2004 yielded major calibration discrepancies for channel 1 and significant ones for channels 2 and 9-11. Subsequently, radiative transfer matchup data were examined for channel 1 and 2. In all cases examined, discrepancies, such as those shown in the left hand panel of Figure 10 for the horizontal polarized (H-pol) calculation, greatly exceeded uncertainties in the radiative transfer calculations for this surface channel (typically +/-5 K). Calculations for V-polarization (V-pol) were in good agreement with SSMIS data. This indicated that SSMIS channel 1 is V-polarized, rather than the specified H-polarization. Smaller polarization-dependent discrepancies were observed for channel 2, which is consistent with the smaller amount of surface emission sensed by this channel. The effect is negligible for channels 3-7 because lower atmospheric emissions are unpolarized. Subsequent examination of hardware components confirmed that channels 1-7 are V-polarized. Similar results were obtained on other days.

5. LATITUDE DEPENDENCE

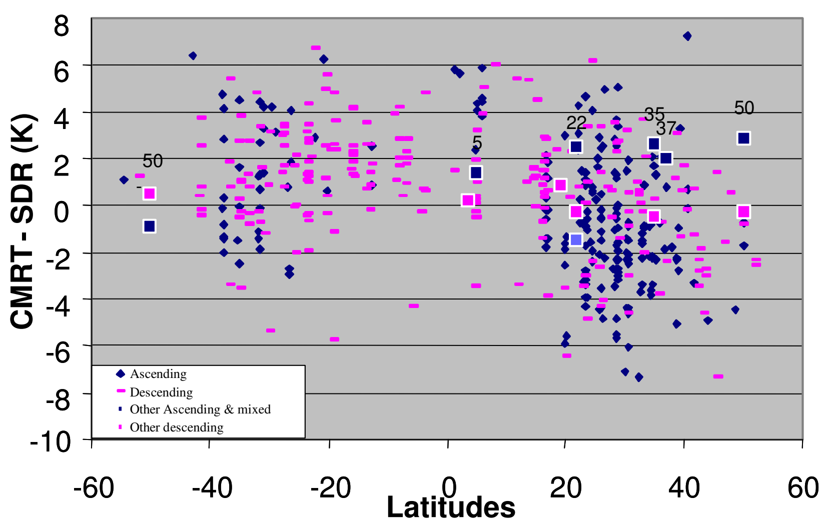

Figure 12. Channel 9 bias versus latitude for operational raobs and special observations.

Key to Special Observations

50S	Worldwide CDFSII Cloud-Screened Raobs 2004 JD 1-365
5N	RV Brown Vaisala RS-90 radiosondes, 27 Oct to 20 Nov 2003. Unscreened average: +1.4 K asc, +0.1 K des, Latitudes from 90W to 110W, Longitudes from 0N to 12N, times from 0 to 23 UTC
19N	WSRP mid-Pacific Dropsondes, NOAA Aeronomy Lab 29 Jan 2004, Latitudes 19N-25N, Longitudes 153W-157W, times 18-20 UT
22N	Barking Sands Lidar Winter '03-'04 (asc), RS-90 radiosondes April '04 (des), Light blue lidar April '04 (asc)
35N	Conus CDFSII screened Raobs
37N	Arm-Cart radiosondes (4)
50N	North Atlantic Dropsondes

Figure 12 compares results for the 183+/-7 GHz water vapor channel obtained from several special measurement campaigns with screened results from operational radiosondes. Results are stratified by latitude. The operational radiosonde data are presented for 2004 JD 17-120 with cloud-screening based on the criterion, Ch 8 |CMRT-SDR| < 7K, pixel-to-pixel RMS <1.5K within a radius of 50 km around the local matchup site. Unaccounted clouds are expected to reduce SDRs relative to CMRT simulations (resulting in positive biases). The special campaign results suggest that biases are different for ascending and descending orbits. Although this is not immediately apparent from the special observation data, the raob data suggest bias may vary with latitude. Seasonal dependence was not recognized at the time the charts were prepared.

Results in Figure 13 for the low altitude temperature channel 3 at 53.6 GHz are similar in many ways to the corresponding chart for low altitude water vapor, channel 9. The operational raob results display appreciable latitude dependence, whereas special observations show differences between ascending and descending orbits. Bias directions appear to be opposite those for channel 9. Channel 3 results exhibit less scatter than channel 9 due to their lower sensitivity to clouds and the higher homogeneity of temperature fields.

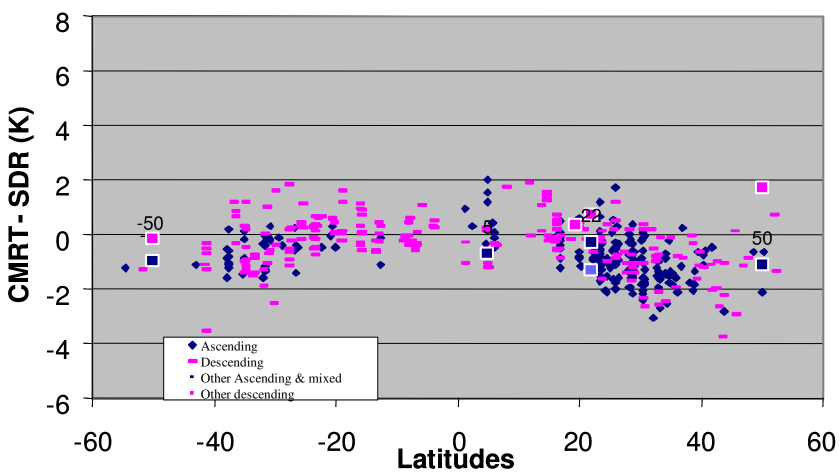

Figure 13. Channel 3 bias versus latitude, operational raobs and special observations.

Cloud Screening: Ch 8 |CMRT-SDR| < 7K, Pixel-to-pixel RMS < 1.5K
Special campaigns are as labeled in the corresponding figure for channel 9
Operational raob data are for 2004 JD 17-122

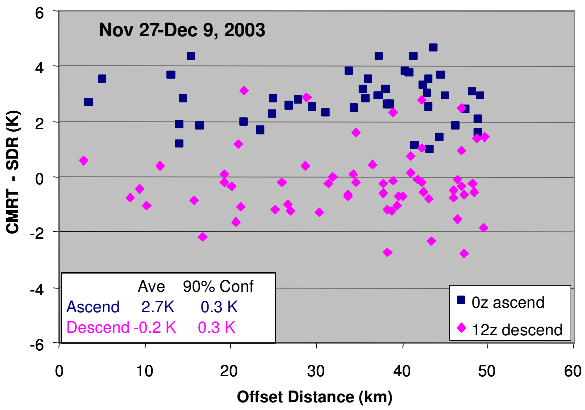

Figure 14. F16 Channel 9 bias based on N. Atlantic dropsondes.

The radiative transfer comparisons shown in Figure 14, based on dropsonde profiles, were obtained from the North Atlantic ATOST-2003 campaign. Flights occurred on 27 November and 8 December 2003 from 44 N to 52 N. During the second campaign, cold dry upper air covered the observation region. This ensures that upper level clouds did not contaminate this set of measurements (ascending evening overpass, dark blue markers). The earlier measurements were made during a morning flight, corresponding to a descending overpass. For about one-half of the descending overpass, relative humidity remained near saturation up to about 300 mb. This may account for the larger spread of descending measurements.

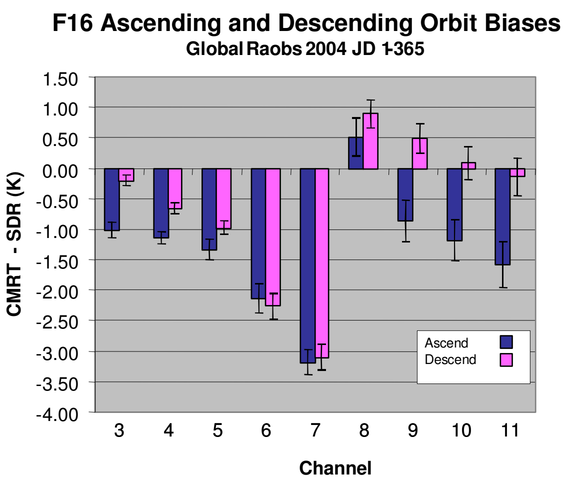

Figure 15. F16 Ascending and descending orbit biases, 2004 global raobs JD 1-365

The yearly global set of synoptic raob-based comparisons (Figure 15, Table 5) shows relatively small, but statistically significant differences between ascending and descending orbit bias measurements. The differences are largest for the water vapor channels and the result suggested that diurnal effects should be considered. Although minor contributions were not ruled out, the magnitude of the effect and the uniformity of ascending/descending bias differences for channels 9-11 were inconsistent with the mechanism. Other evidence, discussed below, identified the likely cause of the orbital dependence as instrumental, rather than environmental. Radiative transfer plus cloud screening should compensate for diurnal effects. Raob-based comparisons were used rather than ECMWF comparisons in these investigations in order to rule out potential contributions from diurnal shifts in ECMWF bias. Unfortunately, typical raob ceilings are 30 km or less and climatology was used for higher altitudes. Therefore radiative transfer estimates for temperature channels 6 and 7 are inaccurate. Solar heating has the potential to bias raob measurements. If this were the case, the effect would be largest for the high altitude temperature channels and should vanish in the low altitude temperature and all water vapor channels. This is contrary to observations. Therefore the global synoptic raob data confirm that instrumental bias changes between ascending and descending orbits. (The large apparent discrepancies for both ascending and descending orbits shown for channels 6 and 7 are not significant because the raob ceiling altitudes are too low to support accurate radiative transfer calculations.)

Table 5. F16 Descending and Ascending Orbit Biases, 2004 Synoptic Raobs JD 1-365

	Descending Orbits				Ascending Orbits			
	Bias (K)	**RMS**	**90%Conf**	**σ**	**Bias (K)**	**RMS**	**90%Conf**	**σ**
3	-0.20	0.81	0.09	0.78	-1.02	1.35	0.13	0.89
4	-0.66	0.98	0.09	0.73	-1.15	1.35	0.10	0.71
5	-0.98	1.38	0.11	0.97	-1.33	1.78	0.17	1.18
8	0.89	2.11	0.22	1.91	0.51	2.22	0.31	2.16
9	0.49	2.11	0.24	2.05	-0.87	2.51	0.33	2.35
10	0.09	2.31	0.27	2.31	-1.18	2.62	0.33	2.34
11	-0.13	2.62	0.31	2.62	-1.58	3.09	0.37	2.66

(All locations, 2004 JD1-365, DMSPC cloud clearing threshold >100%-km, pxl-pxl std dev ch 9 <1.5K, R4 SDR)

Biases for the yearly average meet the derived requirement of +/-1 K for descending orbits. Considering statistical errors, possible systematic errors in both radiative transfer and raob measurements, and differences between the Rev 4 SDRs used above and the corrected Rev 5 SDRs, biases are within measurement error of requirements for ascending orbits. However, the large standard deviations for the water vapor channels confirm the existence of a significant measurement problem.

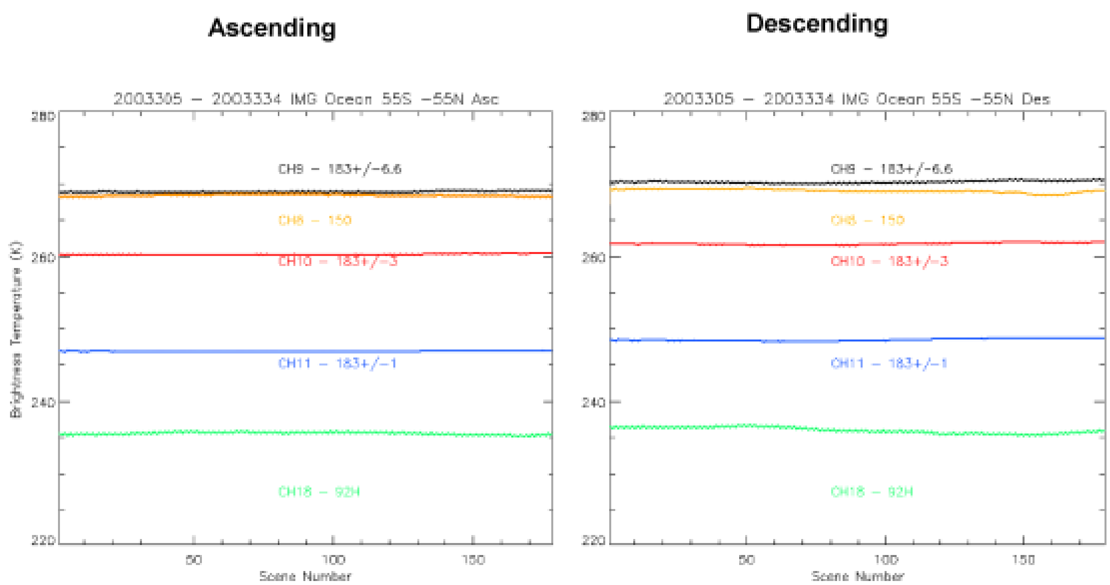

Figure 16. SDRs Globally Averaged Ocean SDRs at 183 GHz.

The data sets shown in Figure 16 were generated by averaging, as a function of scan position (scene number), mid-ocean SDRs from about 50 orbits on days between 2003 JD 305 and 334. Whereas, there is little dependence on scan position, there are significant shifts between ascending and descending orbit averages. Nominally, the same results would be expected for both, given the long averaging period, however the possibility exists that diurnal effects could influence the results, either directly, or by indirectly changing cloud cover.

In the case of SSM/T-2, agreement between ascending and descending orbits, for corresponding oceanic averages, is much better than 1 K. This ruled out diurnal variation as an explanation for the differences shown in Figure 16.

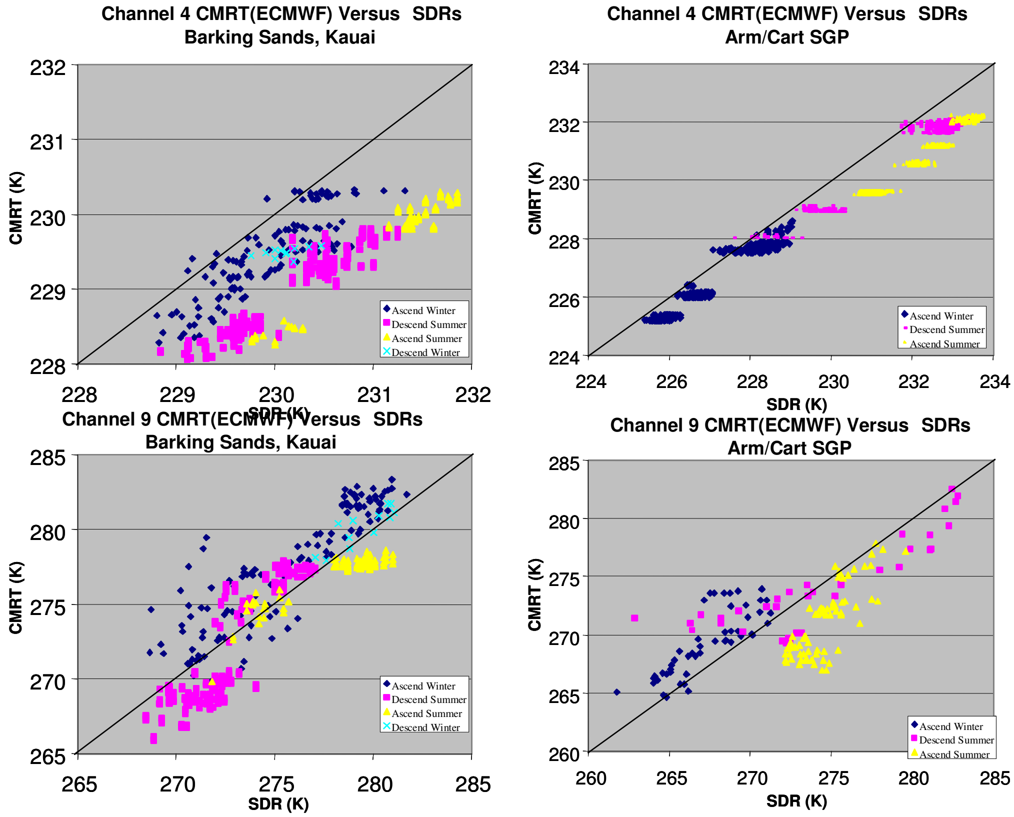

Figure 17. Scatter Plots for channels 4 and 9 stratified by orbit and season.

The scatter plots in Figure 17 of radiative transfer calculations based on ECMWF fields versus SDRs were compiled for Barking Sands and Arm/Cart SGP sites. Data points are separated by season and by ascending and descending orbits. Clearly, summer ascending and winter ascending data show different offsets. In fact, each group has a different offset and the two channels have much different offsets. Clouds may be responsible for cases where channel 9 SDRs spread significantly to cold temperatures, as for example in the panel at lower right for Arm/Cart summer descending SDRs less than 270 K. Differences between ascending winter and ascending summer are greatest. Results for other channels show the same effects, with somewhat less separation and greater scatter. These SDRs are from Rev 5 SDRP.

6. SEASON AND LATITUDE DEPENDENCE OF BIAS

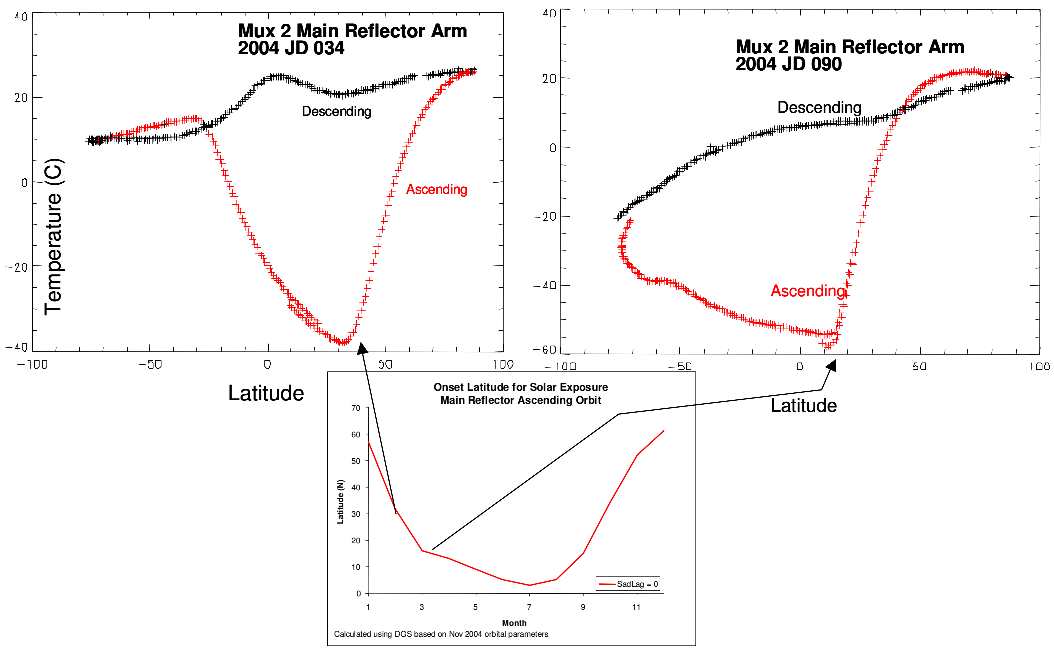

Figure 18. Main reflector arm temperature (Mux2) before and after 2004 JD 41.

The prior results suggested existence of a latitude and possibly season-dependent bias. Subsequent studies indicated that solar heating of the main reflector contributes a changing bias. The graphs shown in Figure 18 aid in understanding when reflector temperature change may influence bias. The effects are most easily observed in water vapor channels 9 and 10 and temperature channels 3-5, which have negligible surface contributions and do not sense appreciably beyond ground truth ceiling altitudes.

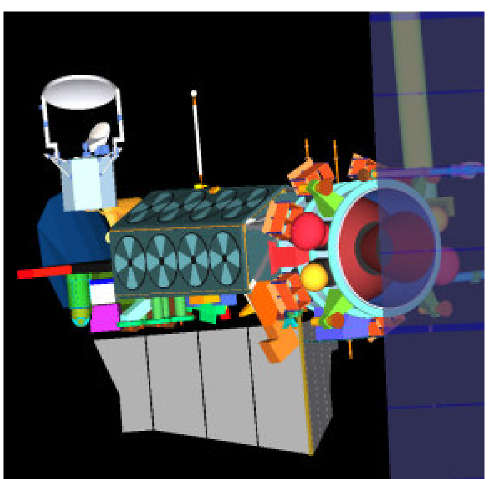

Figure 19. DGS view of SSMIS and F-16 from sun direction.

The on-board temperature sensor closest to the reflector surface is located on the reflector rim. The measurement is designated Mux2. The rim is constructed of the same type of carbon fiber composite material used in the reflector, however the thickness and structural configuration are different. Therefore, this measurement is not expected to portray the reflector surface temperature accurately. However, it does indicate the reflector heating and cooling cycles, although the response is delayed and damped.

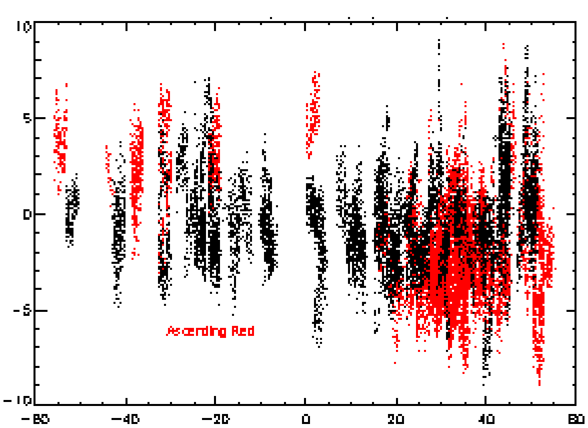

Figure 20. SSMIS Ch 9 bias (ECMWF) versus latitude, 2004 JD 70-90. SSMIS Ch 9 bias (CMRT(ECMWF) – SDR, K) versus latitude, 2004 JD 17-30.

It is instructive to plot a time series of measurements, as shown in Figure 21. These are calculated from monthly averages using CMRT based on operational raobs. (No cloud screen was used.) The lines represent 90% statistical confidence intervals. The data are primarily from CONUS (15N<Lat<45N, N. America) so that the effect of onset of solar exposure in northern hemisphere spring is emphasized for ascending orbits. (The SSMIS solar panel was repositioned on day 41 of 2004. Prior to this, SSMIS was occasionally partially eclipsed by the solar panel, afterward there was no shielding.)

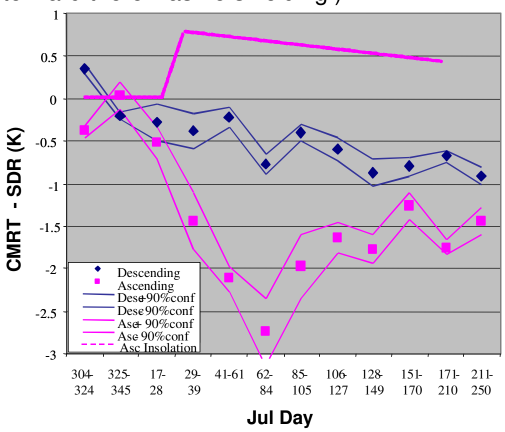

Figure 21. Channel 3 N Hemisphere bias versus day.

Another factor is change of onset latitude for earth eclipse of SSMIS. On average, for CONUS, the transition period ranges over days from about 35 to 60. The dashed magenta line in Figure 21 represents approximate average ascending orbit insolation on the main reflector surface as a function of month over the continental U.S. Surface insolation is maximum in the ascending node at about day 35, slowly decaying to about day 160, then increasing again (not shown) until solar exposure is eclipsed by earth, somewhat after day 300. At day 330 the solar projection on the front reflector nearly vanishes in mid-latitudes for descending orbits. By day 365 exposure gradually increases to a low level. The ascending bias measurements generally track insolation, as shown in Figures 21. Results were similar for the other LAS channels.

SSMIS goes into earth eclipse with a predictable annual pattern. Figure 22 below shows how the pattern varies with month and latitude. The red + symbols indicate the latitude where SSMIS emerges from sun shadow in ascending orbits.

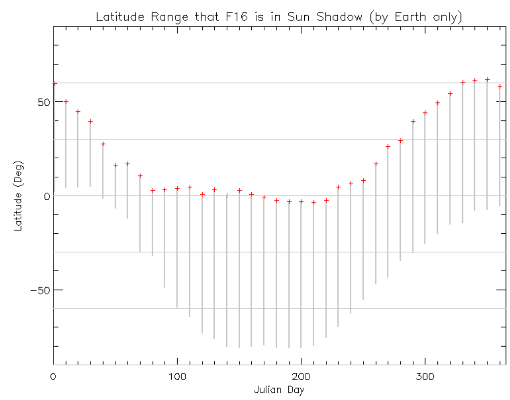

Figure 22. Seasonal dependence of F-16 SSMIS shadow regions for ascending overpasses.

7. BIAS AT SINGLE STATIONS

Time series of bias were examined for various ground stations as a function of season using radiative transfer based on the raob measurements. Results are shown in Figure 23 below for the Barking Sands and Arm/Cart SGP sites, using ECMWF fields. The dashed lines represent approximate trends for ascending and descending orbits. A primary feature of these curves is that bias changes abruptly upon change in solar exposure. The date of the change tracks emergence into or out of solar exposure and has the predicted latitude dependence. SSM/T-1 bias measured at these stations does not exhibit corresponding seasonal dependence, however there is a substantial shift in average bias between the instruments. The same patterns are observed for the SSMIS water vapor channels, however the amplitude of the shifts and the noise levels are increased. All these effects are consistent with bias caused by reflector emissivity

SSMIS CH4: 54.4 GHz F15 SSM/T1 CH3: 54.35 GHz

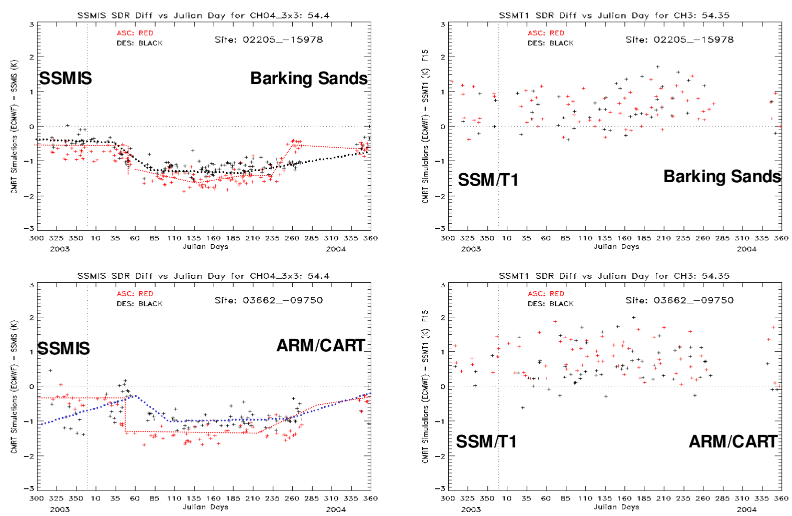

Figure 23. CMRT – SDR calculated based on raobs for channels 3 (right) and 4 (left) as a function of Julian day for the Barking Sands and Arm/Cart SGP sites. Red is for ascending orbit, black is for descending.

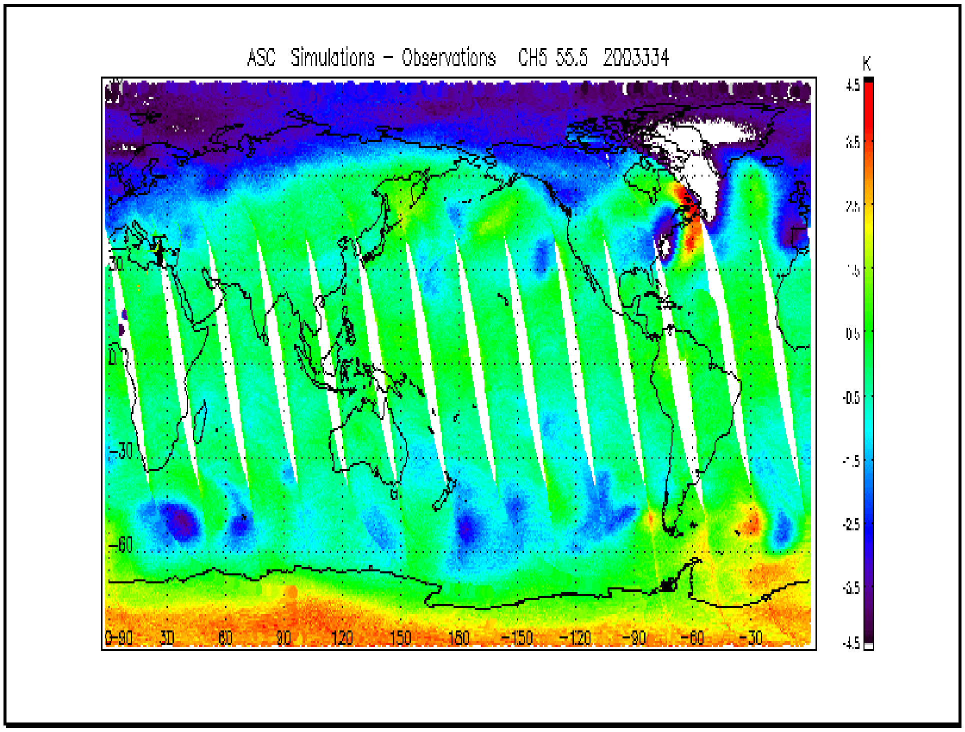

.

Figure 24. Global Bias Channel 5, ECMWF. CMRT - SDRs in ascending orbits, winter 2003 JD 334.

8. Global Simulations

Global simulations also provide compelling evidence for onset of solar-induced bias. Figures 24 was generated using ECMWF fields. Biases are small over mid-latitudes for temperature channels 3, 4, and 5. However, they become large and negative as SSMIS begins ascent into the arctic region. The transition latitude increases from summer to winter. In the case shown above, it occurs, on average, at about 60 N. 60 N corresponds to the latitude where SSMIS emerges from earth shadow during the winter. The transition moves down to the region 0 to 20 N during summer, corresponding to solar onset during that season. Although ECMWF fields are often distorted in regions where major storm systems are active, transition latitude is well defined on a time scale of several days.

Large changes in bias are observed for the moisture channels, however noise levels are increased, presumably due to the influence of unaccounted clouds and higher moisture variability.

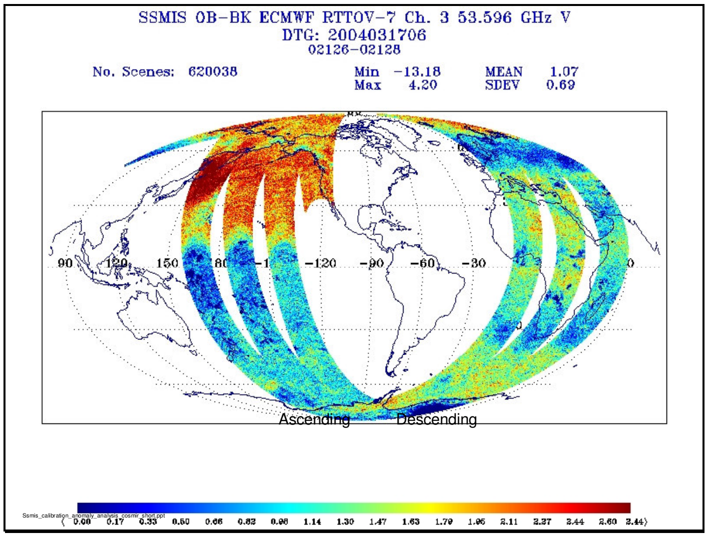

Figure 25. Global bias channel 3, SDR - RTTOV, 17 Mar 2004

Figure 25 represents channel 3 biases for ascending (left hand side) and descending orbits (right hand side) calculated from the difference between SDRs and radiative transfer based on ECMWF fields. Ascending orbit biases are nominal from the south pole up to about 20 N, where solar exposure commences. At higher latitudes, bias increases due to solar heating of the reflector surface. Bias decays in descending orbits as the reflector cools in response to decreasing average solar projection on the front surface. Solar heating of the warm load tines is a major contributor to biases over the southern Atlantic in descending orbits.

9. MODEL FOR SSMIS BIAS DUE TO PRIMARY REFLECTOR EMISSIVITY

The above comparisons between SDRs and radiative transfer calculations (CMRT) demonstrate that sounding channels have variable bias. A simple model for bias contributed by primary reflector surface emissivity (**ε**) indicates that the slope of bias with respect to atmospheric brightness temperature, T_{b0}, is **ε**, and that this bias vanishes when T_b(atm) and the reflector surface temperature (T_s) coincide.

$$T_b(\text{measured}) = (1 - \varepsilon)\, T_{b0} + \varepsilon T_s$$

$$\Delta SDR = T_{b0} - T_b(\text{meas}) = \varepsilon * (T_{b0} - T_s)$$

Analysis is carried out by regressing calculated bias (CMRT – SDR) against SDRs, for time intervals and locations where T_s is uniform. It is assumed that the SDRs are close to (T_{b0}), relative to the range spanned by data points ($T_s - T_b$(atm)), which is about 40 K, and that SDRs are corrected for proportionality factors, such as spillover loss. Biases due to radiative transfer deficiencies and unaccounted clouds are neglected.

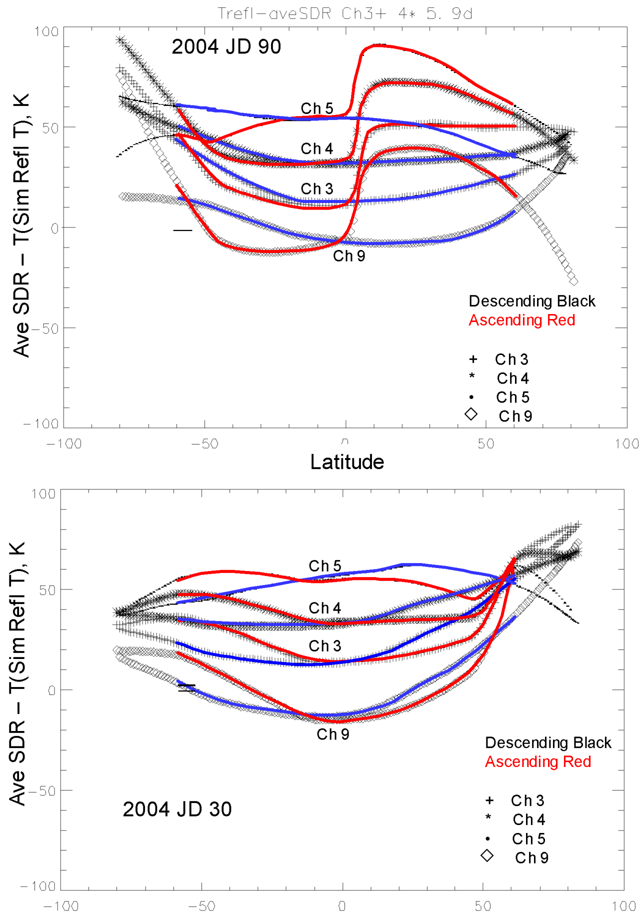

Figure 26. Simulated bias for 2004 JD30 and JD90

An attempt was made to simulate the latitude dependence of emissivity-induced bias for several LAS channels. The reflector surface temperature was crudely simulated using a thermal model involving direct solar heating of the reflector surface and heat loss by conduction to a thermal mass at an average orbital temperature. Solar input to the reflector surface was approximated by graphically (using DGS) to measure the projection of incident sunlight onto the surface. Heating of the rear side of the reflector and radiative heat loss were neglected. Scaling was such that temperatures ranged from 263 to 301 K.

The curves shown in Figure 26 were derived by compiling average SDRs as a function of latitude and subtracting the simulated reflector surface temperature at each latitude. The difference is expected to be proportional to the bias contribution. Major features of the curves indicate that there are extensive regions where bias should be much different in ascending and descending orbits. The vertical scale is likely in error because the actual average reflector surface temperature is unknown. The error is expected to shift the vertical scale. Therefore, vertical offsets will be needed when these curves are compared to data. In addition, a sign change is required for comparisons with the bias plots below.

Figure 27 presents the latitude-dependence of discrepancies between radiative transfer calculations based on raobs and channel 3 SDRs for winter and spring 2004. Red data points correspond to ascending orbit discrepancies (CMRT-SDR), and blue are for descending orbits. Red (ascending) and blue (descending) curves refer to bias predicted by the reflector emissivity model.

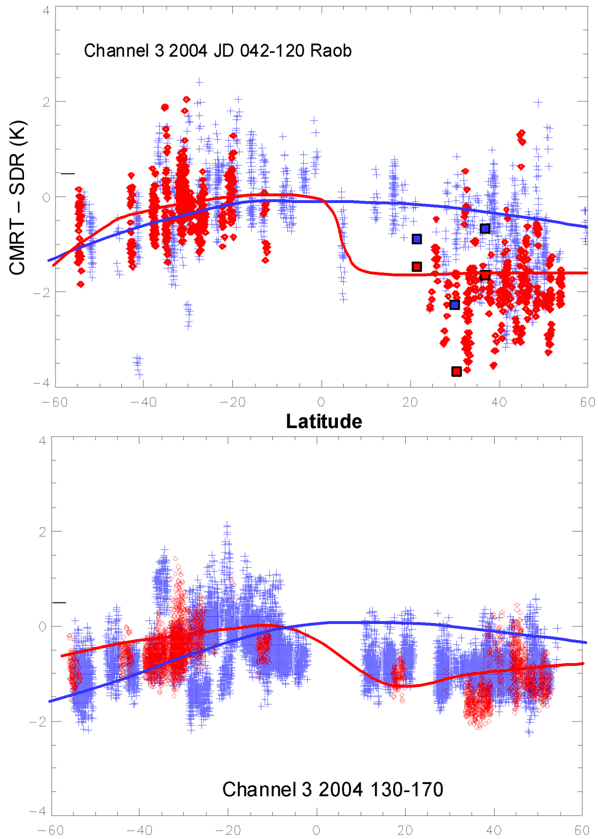

Figure 27. Simulated and observed bias for channel 3 2004 JD 80 and JD 150.

For northern latitudes, the descending model curves are anomalously high relative to measurements, this also applies to channels 4, 5, and 9. Also, the ascending bias correction may decay too rapidly for northern latitudes beyond 20 N. This suggests that the thermal model overestimates heat loss and/or underestimates heating of the back of the reflector. The same effect would lower the ascending bias curve at southern latitudes, thereby improving model agreement. The "high latitude effect" occurs for other channels and seasons.

The reflector emissivity model predicts equal differences between ascending and descending orbit biases for channels 9-11 when observations are confined to a small range of latitudes and times.

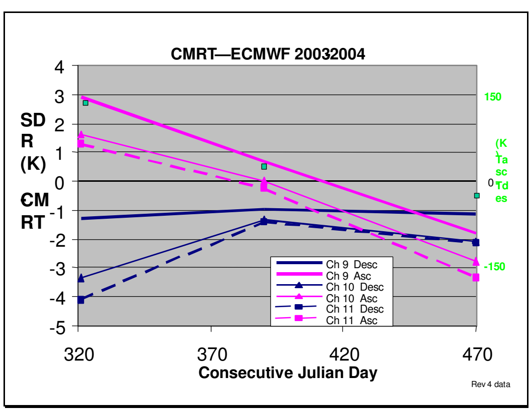

Figure 28. Ascending and descending bias versus day, 2003-2004

In Figure 28, biases were averaged for northern hemisphere locations over the time periods 2003 JD 316-322, 2004 JD 10-40, and 2004 JD 90-120. The green data points are highly approximate estimates of reflector surface temperature differences between descending and ascending orbits (surface temperature difference scale on right hand side). In the first time period, the maximum change in main reflector surface temperature occurs between ascending and descending orbits. As predicted by the model, ascending/descending separations are similar for each channel. The separations decrease substantially for JD 10-40, and there is a slight inversion when, in the last period, the reflector is warmer in the ascending than in the descending node. The above data are fully consistent with the model. A channel-dependent change in bias due to radiative transfer model errors does not alter these considerations, although it would change the displacement between channels. Thus, although displacements between channel 9, 10, and 11 are expected to be similar because the average SDRs differ by about 10K from channel to channel, intervals between channel 10 and 11 curves are less than for channel 9 and 10, suggesting a channel-dependent bias in CMRT.

Statistical errors in the data points range between 0.01 and 0.05 K. The effects of ECMWF and diurnal bias may be larger. The reflector surface temperature change between ascending and descending orbit for 34-50 N on day 320 is expected to be about 140 K. The change in bias implies that surface emissivity is about 0.03 at 183 GHz.

10. SUMMARY OF RESULTS

SSMIS LAS channel biases are relatively small when measured globally for a year, however the standard deviations are large. Without additional information, this suggests either the instrument is noisy, the ground truth measurements have large scatter, or there are geographical, seasonal and/or instrumental drifts. Studies of local biases and deviations confirmed that bias changes with orbit, latitude, and season. Results from all ground truth measurement methods are in accord. Local standard deviations are small. This indicates SSMIS radiometric measurements are locally stable. Calibration data show that biases were present soon after launch and that the bias cycle repeats on an annual basis. This indicates that on-orbit aging is not a major contributor.

Two principal causes have been identified for drifting bias. One is due to solar-induced temperature change of the main reflector surface. Although this surface was designed to have negligible emissivity, such that reflector temperature swings would not cause measurable biases to SDRs, the calibration results indicate that surface emissivity contributes to bias. Measurements from a sample from the SSMIS mass model cold reflector, which nominally has the same type of coating, indicate surface emissivity is nonzero. SIMS surface analyses determined that the multilayer coatings deviate from the expected composition profile, such that SiO_x and Al layers are indistinct. Therefore, it is reasonable to assume that emissivity is higher than intended.

The other source of variable bias is heating of the warm load tines due to solar exposure. This also causes periodic errors in the calibration system.

Mitigation approaches are being implemented to partially correct for warm load related bias perturbations. Measurements and modeling efforts are underway to develop predictive corrections for emissivity-induced bias. The primary needs for F-16 are for accurate measurements of surface emissivity and accurate modeling of reflector surface temperature. The latter is a challenging problem due to the accuracy requirements. For follow-on instruments, the main reflector arm temperature sensor has been relocated near center of the rear surface of the main reflector. This will improve the fidelity of reflector surface temperature estimates.

At this time, there is considerable uncertainty concerning ability to improve F-16 calibration accuracy by implementing bias correction models currently under development. The impacts are modest for the LAS temperature channels and are moderately serious for the water vapor channels. It is anticipated that minor hardware and software modification will provide substantial improvement for follow-on instruments.

11. References

Collins, W. G., 1998 , Coplex quality control of significant level rawinsonde temperatures," J. Atmospheric and Oceanic Technology, 15, 69-79.

Hedin, A. E., Extension of the MSIS Thermospheric Model into the Middle and Lower Atmosphere, J. Geophys. Res., 1991, 96, 1159.

Rosenkranz, P. W., 1998: Water vapor microwave continuum absorption: a comparison of measurements and models , *Radio Science , **33**, 919-928.*

Acknowledgements

This work was sponsored by the Defense Meteorological Satellite Program, United States Air Force, under contract FA8802-04-C-0001.